Characteristics of electromagnetic radiation signal of coal and rock under uniaxial compression and its field application

Xiaofei Liu[1], Zhibo Zhang[2], Enyuan Wang[1,*], Xiaoran Wang[1], Bo Yang[1] and Hao Wang[1]

[1]*Key Laboratory of Gas and Fire Control for Coal Mines, School of Safety Engineering, State Key Laboratory of Coal Resources and Safe Mining, China University of Mining and Technology, Xuzhou 221 116, Jiangsu, China.*
[2]*School of Civil and Resource Engineering, University of Science and Technology Beijing, Beijing 100 083, China.*
Corresponding author. e-mail: weytop@cumt.edu.cn   cumtweytop@163.com

Rockburst is a serious threat to the safety and efficiency of coal-mine production in China. Accurate monitoring and prediction of rockburst is an ongoing challenge in coal mining. Electromagnetic radiation (EMR) technology is a real-time and non-contact prediction method for changes in the mechanical parameters of coal or rock. In this paper, uniaxial compression testing of coal and rock samples was carried out, EMR data were collected and analysed from deformation to failure. The rescaled range (R/S) analysis method was applied to study the Hurst index of the EMR signals during the uniaxial compression test. The results showed that the higher the degree of deformation and failure, the larger the Hurst index. On the basis of the experimental and theoretical results, the Hurst index of the EMR signal during the '8.11' rockburst in the Yuejin coal mine was analysed. The results showed that the Hurst index was low before the rockburst, and increased to 0.9 in the pre-rupture stage, then decreased 1–2 days before the rockburst. This suggests a correlation between EMR and the conditions leading to a rockburst event. Therefore, further study on the characteristics of EMR can contribute to development of early-warning technology for rockburst.

Keywords. Rockburst; coal and rock; deformation; failure; electromagnetic radiation; Hurst index.

1. Introduction

Rockbursts are serious geological dynamic disasters which occur in coal mines. Rockbursts can lead to a spontaneous and violent failure of the coal or rock mass, which releases large amounts of elastic energy, rock or coal lumps into the tunnel (the comparisons of roadway before and after a rockburst disaster are shown in figure 1), injuring workers and damaging equipment and facilities (Jiang *et al.* 2014; Liu *et al.* 2017). China has been one of the most seriously affected countries in the world, with many rockburst disasters occurring since the first disaster in 1933. As mining depth increases, underground engineers face more challenging geographical environments with extreme conditions such as high crustal stress, high geo-temperature, high seepage pressure, and strong disturbance under the influence of mining (He *et al.* 2005; Wang *et al.* 2017a, 2018b). In such geographical regions, the occurrence frequency and intensity of rockburst disasters have been

(a) before   **(b)** after

Figure 1. Comparison of roadway before and after a rockburst disaster.

increasing in recent years. Therefore, monitoring and early-warning of rockburst in deep mines have become important issues facing researchers and mining engineers.

Through long-term studies of coal and rock dynamics, researchers have proposed some traditional methods and indexes for rockburst risk assessment and prediction of rockbursts in coal mines, such as bursting liability indices, drilling cutting method, roof displacement and mining-induced pressure measurement (Jiang *et al.* 2014). With the development of data acquisition and signal processing technologies, some geophysical methods for detecting rock instability have emerged, such as acoustic emissions testing (Wang *et al.* 2017b, 2018b; Zhang *et al.* 2017, 2018), ultrasonic testing (Sun and Zhu 2014; Zhang *et al.* 2016, 2019; Wang *et al.* 2018a), infrared thermal imaging (Li *et al.* 2018), microseismic testing (Lu *et al.* 2013; Jiang *et al.* 2017) and electromagnetic radiation (EMR) (Li *et al.* 2016; Liu *et al.* 2018). Initially, scholars studied the phenomenon of abnormal EMR before earthquakes (Eftaxias *et al.* 2003). Then, EMR was used to predict deformation and failure of loaded rock (Lichtenberger 2005; He *et al.* 2010). Because EMR technology can reflect the evolution of rock fracture, it is receiving increasing attention from researchers (Dov *et al.* 2001; Mastrogiannis *et al.* 2015).

Many studies have assessed the risk of rockburst in coal mines. By analysing a large amount of monitoring data from coal mines, Frid *et al.* (1992, 1997) showed the correlation between EMR intensity and the risk of rockburst occurrence under high stress, and described quantitatively the risk level of rockburst ahead of the mining face by using EMR pulses. He *et al.* (2002) and Wang *et al.* (2014) carried out further studies on EMR signals

recorded during deformation and failure of coal and rock and analysed the EMR characteristics. Rabinovitch *et al.* (2017) calculated the directionality of EMR from tensile fracturing, and constructed a theoretical model which agreed with field observations. Because EMR is emitted in the developmental stages (between hours and days before the collapse occurs) of rock or coal collapses in mines (Leeman *et al.* 2014; Balasco *et al.* 2015), detection of EMR may provide a warning of rockburst occurrences. Theoretical models and technological developments that can be applied to rockburst prediction by EMR analysis have been recently formed. Song *et al.* (2017) found that pre-rockburst EMR indicators such as its intensity and number of pulses are well and positively correlated. A time-series data mining and group identification system based on pre-rockburst EMR was developed by Liu (2008), which improved the accuracy of EMR technology to predict dynamic coal and rock disasters.

Although EMR technology has been widely applied in Chinese coal mines and achieved good results, our understanding of the general characteristic of EMR in each stage of the deformation and failure of coal and rock and its evolution process is still lacking. In this study, we recorded and analysed the EMR signal emitted from coal and rock samples undergoing deformation and failure under uniaxial compression. On the basis of the stress–strain curve of the coal and rock, the process of deformation and failure was divided into stages according to the energy characteristics of the EMR signal. Moreover, to provide a theoretical basis for monitoring rockburst in coal mines using EMR technology, the EMR signal of a high-risk mining face area was recorded and its response during rockburst evolution was analysed.

2. Experimental system for detecting EMR in coal and rock under uniaxial loading

Here, we present the experimental system which was used to monitor the EMR signal of coal and rock samples under uniaxial compression.

2.1 *Experimental system*

The experimental system consisted of a loading system and EMR signal acquisition system (figure 2).

The YAW4306 electro-hydraulic servo press (produced by MTS-SANS Shenzhen Operations) was used in the experiment. Its maximum load is 3000 kN. The test force resolution and relative error are 1:300000 and ±1%, respectively. The loading rate is 0.6 N/s to 60 kN/s with a precision of ±1%. The press machine has two control modes, the force control mode and the displacement control mode. It can carry out various mechanical experiments, such as uniaxial compression tests, cyclic loading tests, and creep tests. The PCI-II acoustic emission acquisition system (produced by Physical Acoustics Corporation) was used to receive the EMR signals. The peak frequency of the EMR sensor is 800 Hz.

2.2 *Samples*

The coal and rock samples were from the Taoshan coal mine, where rockburst has occurred. The coal samples were raw coal samples taken from the coal block and processed to produce cylindrical samples (measuring Φ, 50 mm × 100 mm) in accordance with the standards of the International Society for Rock Mechanics. The parameters of samples, including size, shape, species and the loading rate, are shown in table 1.

3. Analysis of the EMR signals

3.1 *EMR signals of coal and rock under uniaxial compression*

The number of EMR pulses (EMR pulse count) and the energy of the rock samples under uniaxial compression are shown in figures 3 and 4. The EMR pulse count and the energy increased with increased loading. In the initial loading stages, the integrity of the rock samples increased as the pre-existing fissures were compacted, resulting in a low EMR pulse count and low energy. As the load increased, new cracks appeared and expanded gradually. This caused the EMR pulse count and energy to rise significantly. When the load is increased further, the rock fractured and the EMR pulse count and energy reached their maximum values.

The change in the EMR pulse count and energy of the coal samples under uniaxial compression is shown in figure 5. The EMR pulse count and the energy of the raw coal samples had good consistency with the load. The EMR pulse count and energy of the coal samples were lower than those of the rock samples. Moreover, the EMR pulse count and energy reached their maximum when the coal fractured and rapidly released the accumulated stress.

In the initial loading stage (AB Stage) the coal and rock samples show elastic properties (figure 6). The samples accumulate elastic potential energy, and do not fracture under load; the EMR signal is weak. When the load exceeds a certain value,
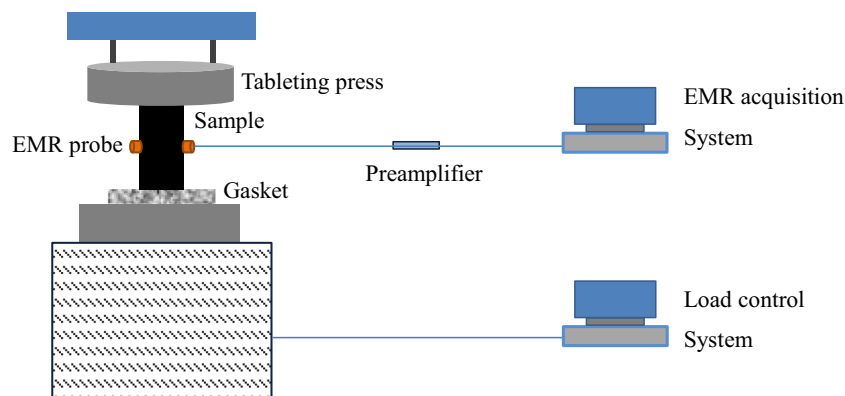

Figure 2. Schematic diagram of experimental system.

Table 1. *Experimental parameters of coal and rock samples.*

Number	Samples	Species	Size (mm)	Loading rate (mm/min)
1#	Rock of roof	Siltstone	Cylinder Φ 50 × 100	0.2
2#	Rock of roof	Fine sandstone	Cylinder Φ 50 × 100	0.2
3#	Raw coal	Burst coal	Cylinder Φ 50 × 100	0.2

(a) Load curves

(b) EMR pulse count   **(c)** EMR energy
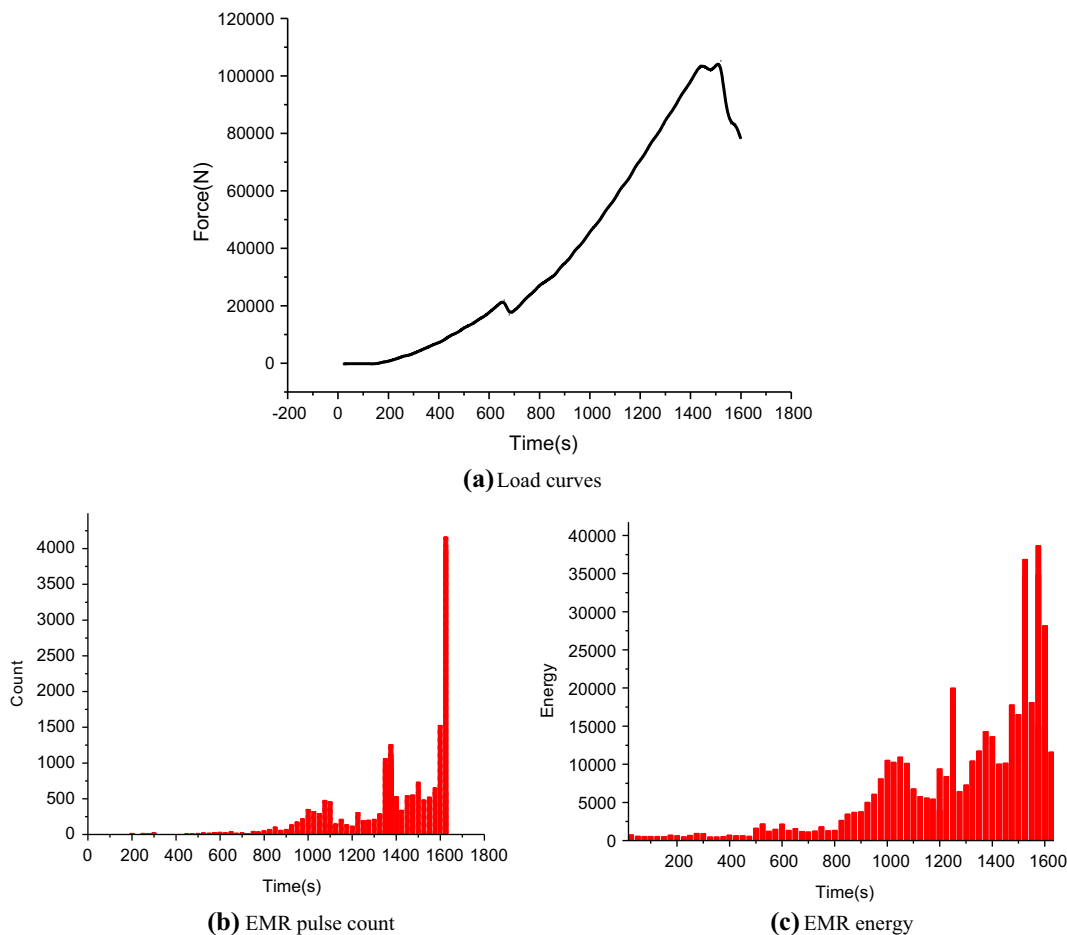
Figure 3. Experimental result of 1# rock sample under uniaxial compression.

pre-existing fissures start to expand and coalesce and some cracks begin to appear. The coal and rock samples undergo plastic deformation that cannot be recovered. The EMR pulse count and energy increase significantly in this stage (BC Stage). When the coal and rock fail, the EMR pulse count and energy reach their maximum value (CD Stage). Thus, the EMR pulse count and energy can reflect the degree of coal and rock failure.

3.2 *Hurst index of the EMR energy of coal and rock*

The Hurst index was introduced by the British hydrologist H E Hurst. The Hurst index is

calculated using the rescaled range (R/S) analysis method which can be used in most time series (Price and Newman 2001; Chen and Chen 2005; Ni and Liu 2005). Wang *et al.* (1998) have found that the EMR signal of coal is in accordance with the R/S statistical law. R/S statistics is used to study the underlying structure of underground zones (Wang *et al.* 2008).

We define the time sequence of the EMR signals as:

$$\{x(t)\}, \quad t = 1, 2, \ldots, N. \tag{1}$$

The EMR time series is divided into A subintervals of length n (the last subinterval may be shorter than n). $\Phi_a, a = 1, \ldots, A$ is used to

(a) Load curves
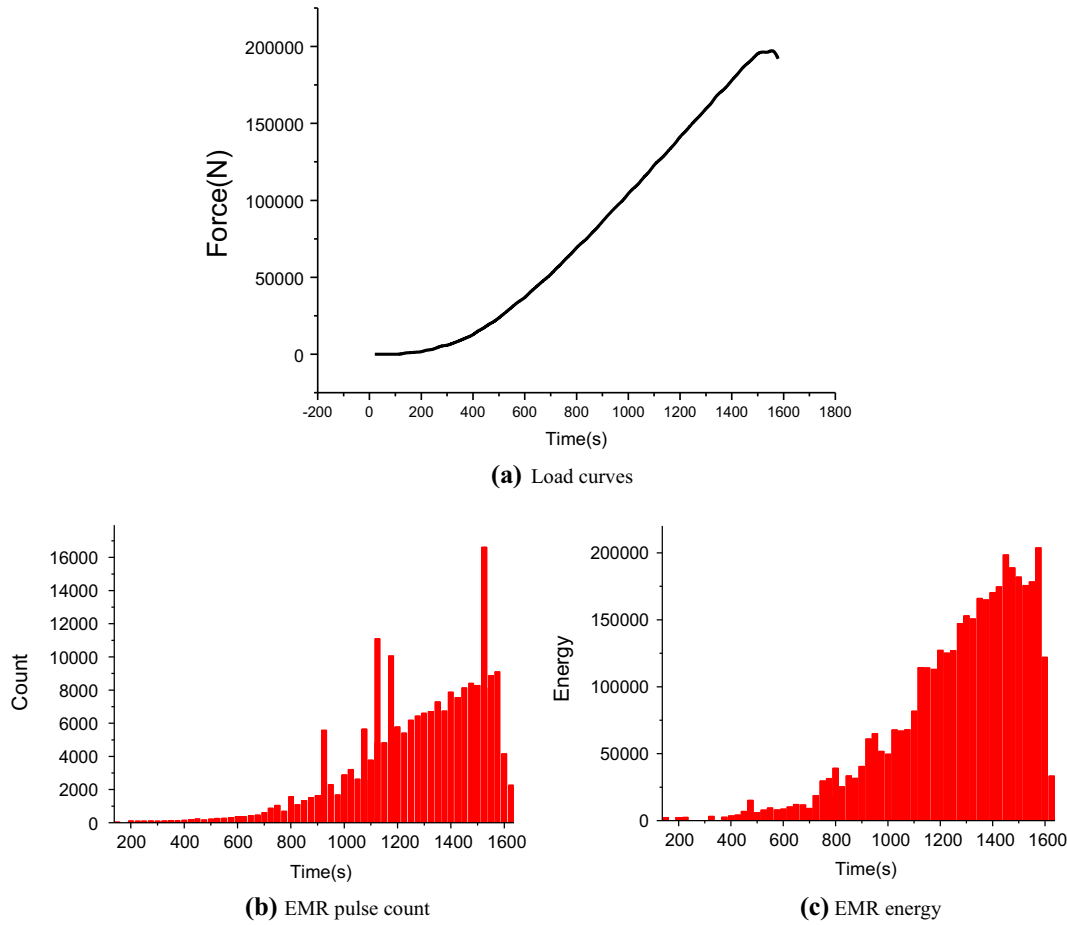

(b) EMR pulse count

(c) EMR energy

Figure 4. Experimental result of 2# rock sample under uniaxial compression.

represent each subinterval, and every point in Φ_a can be represented as $R_{k,a}, k = 1, \ldots, n;\quad a = 1, \ldots, A.$

For subinterval Φ_a of length n, its average sequence is defined as:

$$\langle X \rangle_n = \frac{1}{n} \sum_{t=1}^{n} x(t) = \frac{1}{n} \sum_{k=1}^{n} R_{k,a}. \quad (2)$$

$X_{(k,a)}$ is represented as the accumulated deficiency in the subinterval:

$$X_{(k,a)} = \sum_{i=1}^{k} \left(R_{i,a} - \langle X \rangle_n \right) \quad k = 1, 2, \ldots n. \quad (3)$$

According to equation (3), the sum of the accumulated average deviation sequence $\left\{ X_{1,a}, X_{2,a}, \ldots, X_{n,a} \right\}$ is zero.

R_{Φ_a} is used to represent the range of each subinterval:

$$R_{\Phi_a} = \max_{1 \leq k \leq n} X(k, a) - \min_{1 \leq k \leq n} X(k, a). \quad (4)$$

The standard deviation S_{Φ_a} is used to calculate the rescaled range R_{Φ_a}/S_{Φ_a}:

$$S_{\Phi_a} = \sqrt{\frac{1}{n} \sum_{i=1}^{n} \left[x(i) - \langle X \rangle_n \right]^2}. \quad (5)$$

Therefore, for a subinterval of length n, the average rescaled range of A subintervals is calculated as

$$(R/S)_n = \frac{1}{A} \sum_{a=1}^{A} \left(\frac{R_{\Phi_a}}{S_{\Phi_a}} \right). \quad (6)$$

The relation between the rescaled range and the Hurst index H can be expressed as:

$$\frac{R}{S} \sim (n)^H. \quad (7)$$

For different lengths n, different average rescaled ranges can be calculated through circular computations. Mandelbrot (1999) proved that $\log(R/S)$ and $\log(n)$ have a linear relationship:

$$\log(R/S)_n = b + H * \log(n). \quad (8)$$

A double logarithmic regression is used for n and R/S. The slope of the line in equation (8) is the

(a) Load curves

(b) EMR pulse number
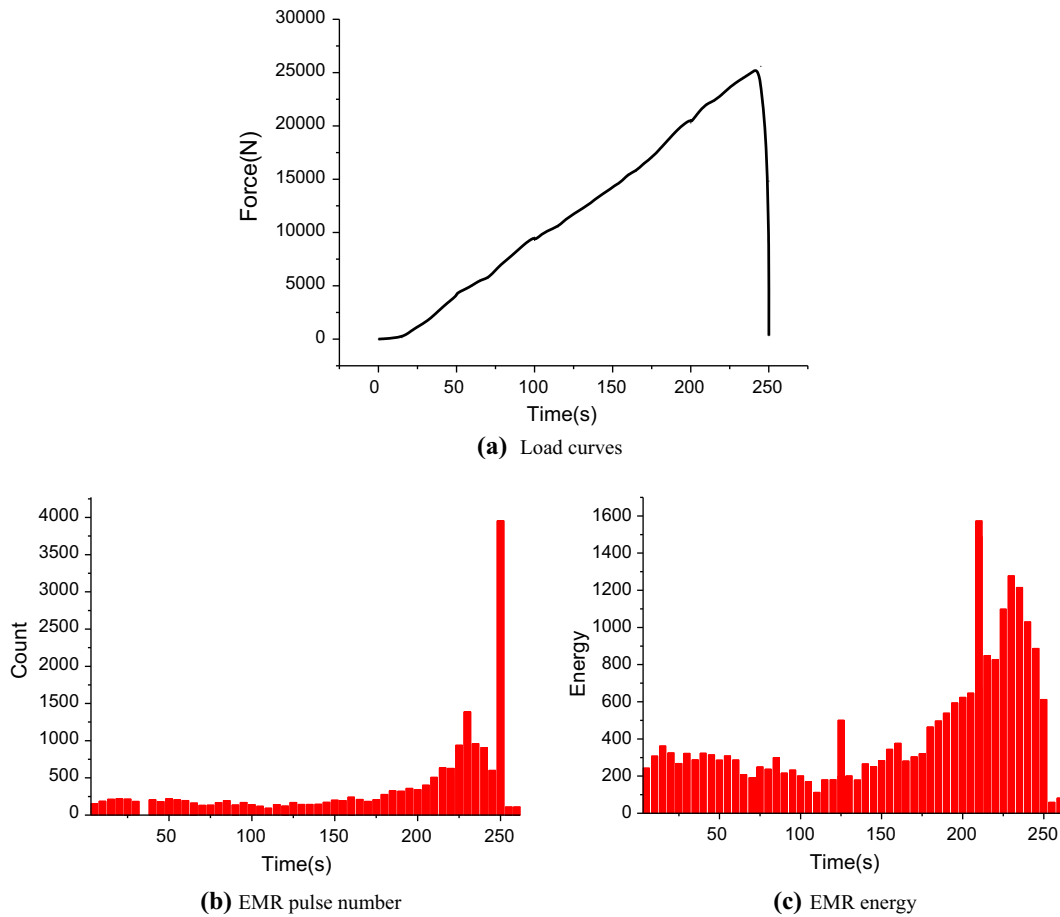

(c) EMR energy

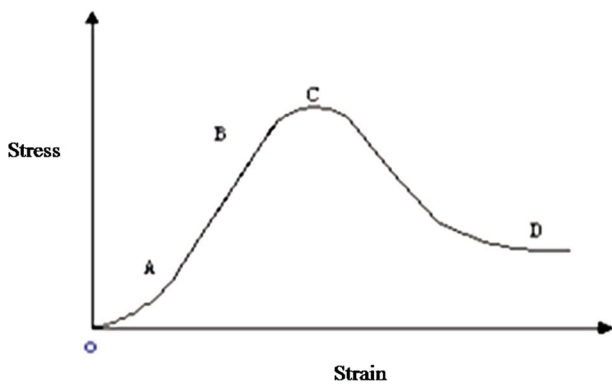Figure 5. Experimental result of 3# raw coal under uniaxial compression.

Figure 6. Stress-strain curve of coal and rock deformation and fracture.

long-range correlation parameter H (the Hurst index). Least squares analysis is used to obtain the parameters of the long-range correlation sequence.

MATLAB software was used to create the program for calculating the Hurst index of the EMR in each stage of loading.

Although there were differences between the EMR variation in the coal and rock samples under uniaxial compression, the overall trend was similar. For brevity, we only show the Hurst index of the EMR energy of the raw coal under uniaxial compression (figure 7). As shown in table 2 and figure 8, H of the EMR energy increases with increasing coal deformation. When the loaded coal is in the initial deformation stage (0–175 s), the EMR energy is low and H is small. In the pre-rupture stage (175–250 s), H increases. According to the calculation, H of the EMR energy of the coal samples in the pre-rupture phase increases by 17% relative to its value in the initial deformation stage.

Rockburst is a result of fractures forming in the coal and rock mass around the outburst area. A sudden drop in the compressive strength of the coal and rock occurs because of the stress concentration in the coal and rock, which results in fracture. This releases elastic potential energy in the coal and rock, creating instability in the roof and floor of the coal seam which causes the rockburst. Thus, the rockburst is a result of the development of fractures in the coal and rock mass around the outburst area. The coal and rock fracturing process in the
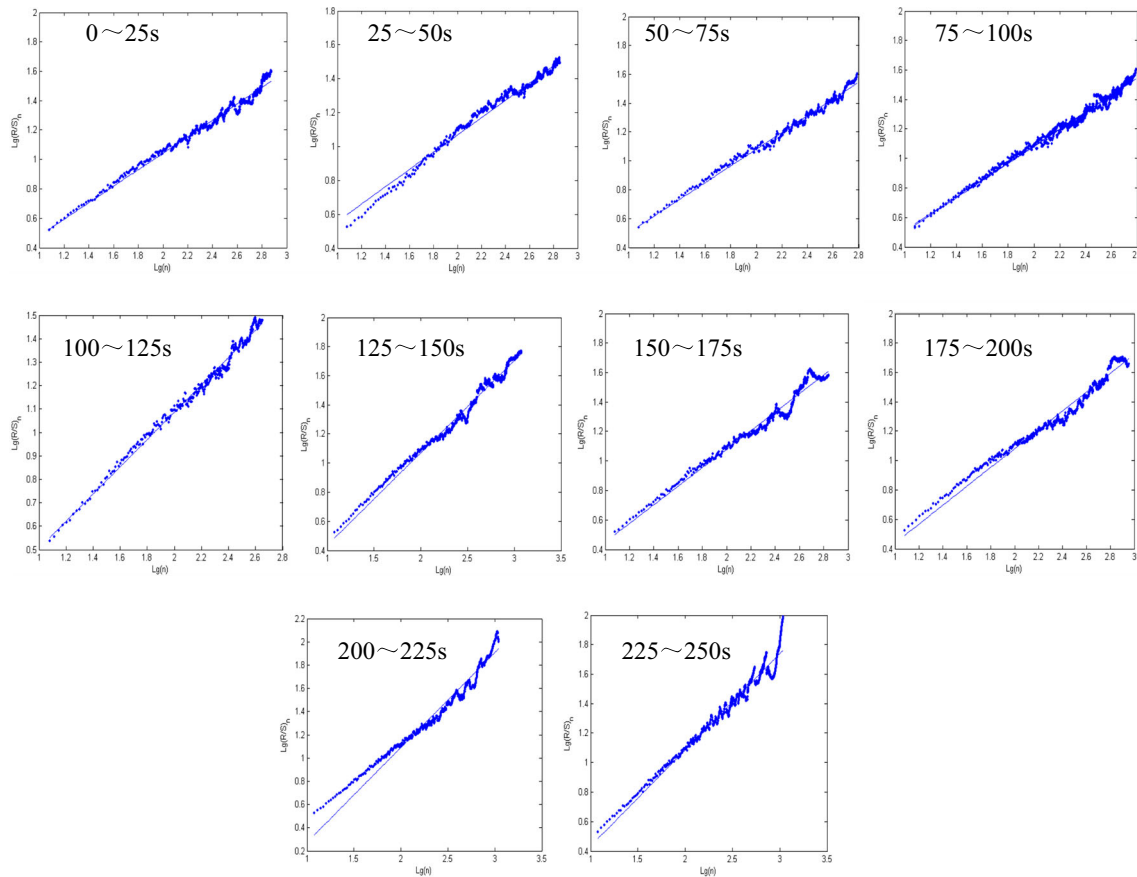
Figure 7. Hurst index distribution of EMR signals of 3# raw coal.

Table 2. *Statistics Hurst index distribution of EMR signals of 3# raw coal.*

Time (s)	0–25	25–50	50–75	75–100	100–125
Hurst index	0.5601	0.5089	0.5796	0.5762	0.5821
Time (s)	125–150	150–175	175–200	200–225	225–250
Hurst index	0.6226	0.6281	0.6254	0.6389	0.8158

laboratory uniaxial loading experiment is similar to the process leading to rockburst in the coal mine. Through studying the changes in energy levels in the coal and rock samples via EMR signals at different loading stages, we can infer on the general characteristic of EMR in the evolution of rockburst.

4. Field case study of a rockburst disaster

4.1 *EMR monitoring device*

In the field observation, we used portable KBD5 EMR equipment which has strong anti-interference capabilities (figure 9a). It has been widely used for monitoring and recording the early-warning signs of rockburst disasters in coal mines and ore mines in China (Li *et al.* 2016). The KBD5 equipment

comprises an EMR data acquisition system, EMR data processing system, broadband frequency (1–500 kHz), a highly sensitive magnetic loop antenna, and a built-in power supply. The KBD5 device can monitor continuously for 6 hrs and has many advantages. For example, the device is intrinsically safe and weighs only 3 kg, so can be easily carried in narrow tunnels in underground coal mine. The effective monitoring range is approximately 7–22 m and its effective directional range is up to 60°. The receiver's frequency bandwidth is 1–500 kHz, and the signal-to-noise ratio is ≥6 dB.

4.2 *Layout of measuring points*

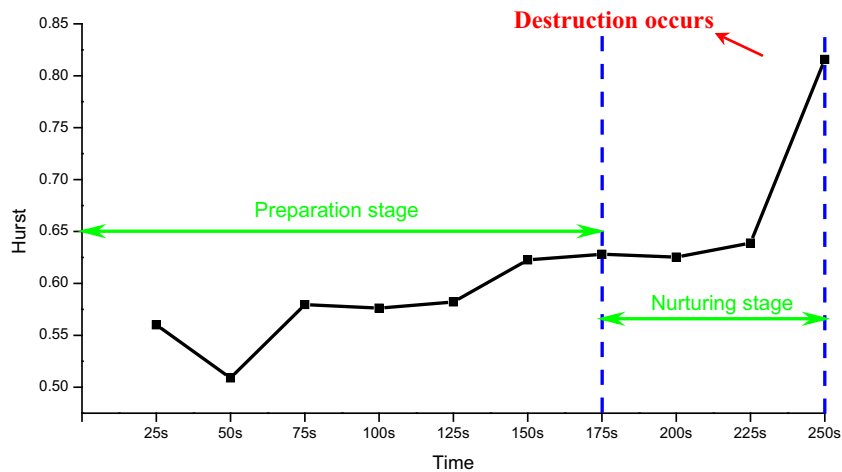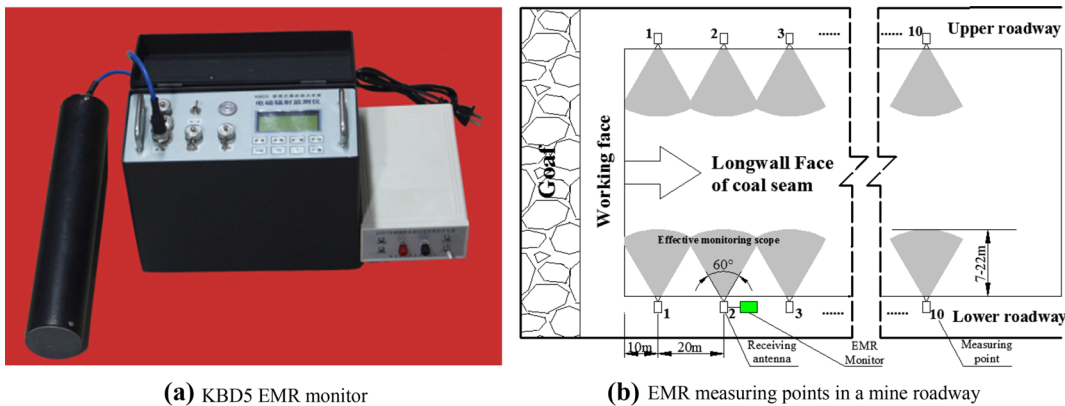The EMR monitoring area was within 200 m in front of the working face (figure 9b). Twenty

Figure 8. Hurst index change trend of EMR signals of 3# raw coal.

(a) KBD5 EMR monitor

(b) EMR measuring points in a mine roadway

Figure 9. EMR monitoring device and measuring points layout.

measuring points were set: ten at the upper road-way and ten at the lower roadway. The distance between each monitoring point was 20 m and the first point was located 10 m ahead of the working face. For each point, the test lasted 2 minutes and real-time monitoring data were collected and saved automatically.

From the recorded EMR wave data, we extracted EMR parameters such as energy, pulse count, frequency, and amplitude through the KBD5 software (Wang *et al.* 2014). These parameters were used in the early-warning method (such as the critical value method or trend method) to assess the rockburst risk at the monitoring site. The addition of the Hurst index into the KBD5 software, as proposed in section 2.2, should improve the automatic rockburst early-warning systems in coal mines and prevent disasters.

4.3 *Case study of the '8.11' rockburst disaster*

At 18:00 on August 11, 2010, a rockburst occurred in the Yuejin coal mine at working face no. 25110 when a *M* 2.7 earthquake struck the region, releasing 9×10^7 J of energy. The rockburst damage extended from the end of the tunnel to a point 300 m from the working face.

The field monitoring at the study site shows that on July 30, 2010 a rockburst event occurred at the same area. This rockburst caused differing degrees of rib spalling within an 80-m range ahead of the working face. During the rockburst, the outburst source and the coal and rock surrounding the tunnel showed a range of responses, from deformation to failure, accompanied by inner energy changes from energy accumulation to energy release. After the rockburst, the coal and rock
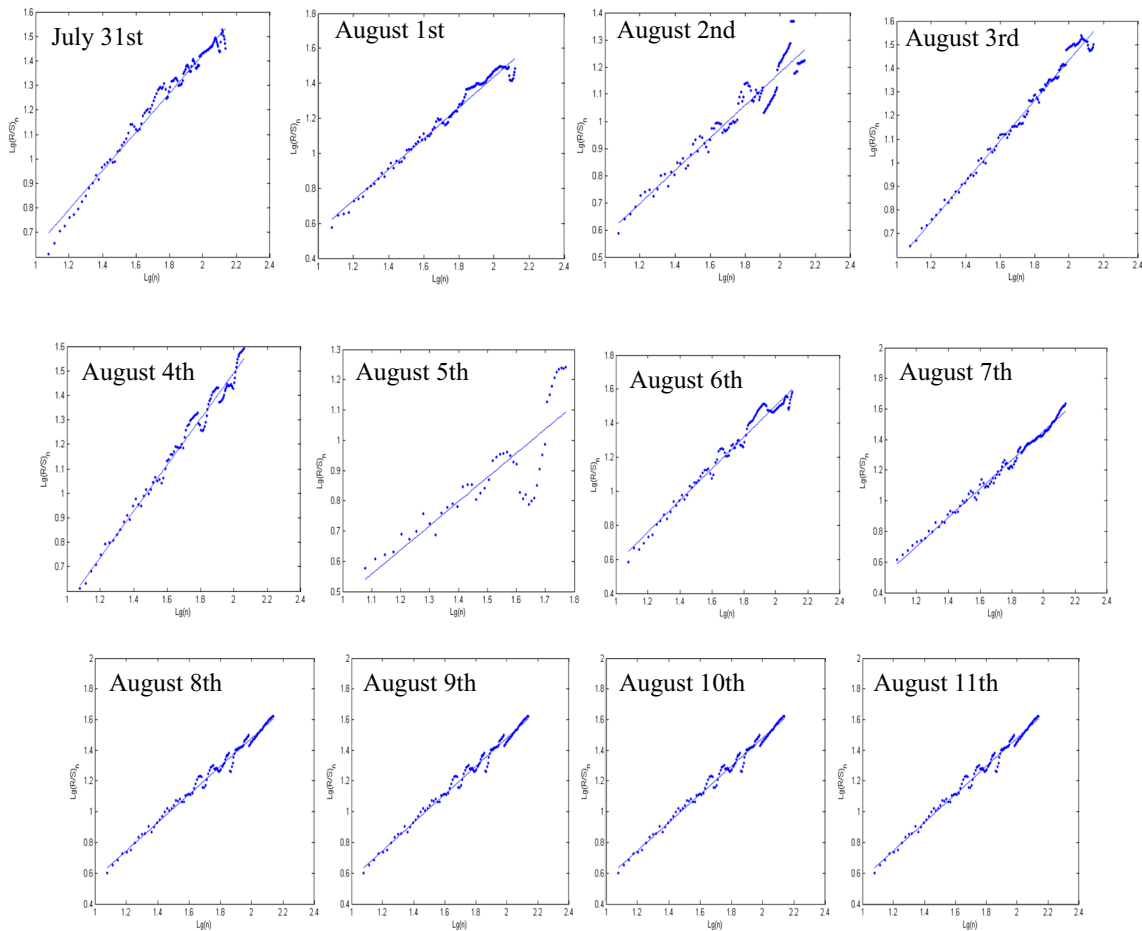
Figure 10. Hurst index distribution of EMR signal of '8.11' rockburst before 11 days.
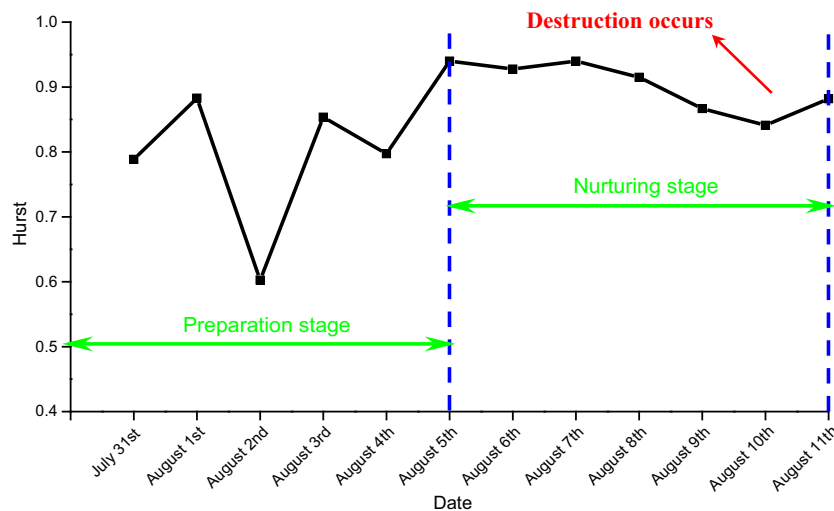

Figure 11. Hurst index change trend of EMR signals of '8.11' rockburst before 11 days.

around the area exhibited the same response again until the next rockburst occurred.

The distribution of the EMR Hurst index in the 11 days preceding the '8.11' rockburst is shown in figure 10. A moving average analysis performed on

the H data shows that the EMR Hurst index around the outburst area increased significantly before the rockburst (figure 11 and table 3). Eleven days before the rockburst, H was small, but as the energy in the coal and rock and the degree of coal

Table 3. _Statistics Hurst index of EMR signal of coal burst before 11 days._

Date	July 31st	August 1st	August 2nd	August 3rd	August 4th	August 5th
Hurst index	0.7886	0.8829	0.6027	0.8536	0.7972	0.9400
Date	August 6th	August 7th	August 8th	August 9th	August 10th	August 11th
Hurst index	0.9277	0.9400	0.915	0.8667	0.8411	0.8819

and rock deformation increases, H tends to rise. Six days before the rockburst, H reached 0.9 then slowly dropped until the day before the rockburst.

The changes in the H of the EMR energy field revealed in this study indicate that the dynamic evolution of coal and rock burst events can be detected by monitoring the EMR energy emitted from the coal and rock surrounding the rockburst site. On the basis of our laboratory test results, the rockburst evolution can be divided into two stages: the initial deformation stage and the pre-rupture stage.

5. Conclusions

(1) Laboratory tests were conducted to record the EMR signal during the deformation and failure of coal and rock samples under uniaxial compression. Analysis of the test results shows that the coal and rock deformation and failure processes were accompanied by changes in the EMR signal and its Hurst index. At the preliminary stage of loading, the coal and rock remained stable and could bear the inner energy; hence, the EMR energy dissipation was low. As the load increased, the deformation reached its threshold value, at which point the coal and rock could no longer bear the accumulated energy; the inner energy was released suddenly and the dissipation of EMR energy increased quickly, reaching a peak when the rock damage was complete. The experimental results show that the dissipation of EMR energy can reflect the drop of the coal and rock strength.

(2) The Hurst index of the EMR energy emitted during the deformation and failure of raw coal under uniaxial compression was derived. The EMR H became larger as the coal and rock failure intensified. In the pre-rupture phase, H increased 17% relative to its value in the initial deformation phase.

(3) The R/S statistical analysis method was used to study the EMR H of the '8.11' rockburst. It showed that the EMR signal of the rockburst

has poor long-range correlation in the initial deformation phase. However, when the rockburst was in the pre-rupture phase, the long-range correlation increased, reaching about 0.9. H dropped 1–2 days before the rockburst.

References

Balasco M, Lapenna V, Romano G, Siniscalchi A, Stabile T A and Telesca L 2015 The Pollino 2011–2012 seismic swarm (southern Italy): First results of the ML=3.6 aftershock recorded by co-located electromagnetic and seismic stations. _Boll. Geofis. Teor. Appl._ **56(2)** 203–210.

Chen Y and Chen L 2005 Fractal geometry, Seismological Press, Beijing.

Dov B, Avinoam R and Frid V 2001 Fracture characterization of chalk in uniaxial and triaxial tests by rock mechanics fractographic and electromagnetic radiation method; _J. Struct. Geol._ **23** 1531–1547.

Eftaxias K, Kapiris P, Polygiannakis J and Peratzakis A 2003 Experience of short term earthquake precursors with VLF–VHF electromagnetic emissions; _Nat. Hazard Earth Syst._ **3(3)** 217–228.

Frid V 1997 Rockburst hazard forecast by electromagnetic radiation excited by rock fracture; _Rock Mech. Rock Eng._ **30** 229–236.

Frid V, Shabarov A N, Proskuryakov V M and Baranov V A 1992 Formation of electromagnetic radiation in coal stratum; _Sov. Min. Sci._ **28** 139–145.

He M C, Xie H P, Peng S P and Jiang Y D 2005 Study on rock mechanics in deep mining engineering; _Chin. J. Rock Mech. Eng._ **24(16)** 2803–2813.

He X, Chen W, Nie B and Zhang M 2010 Classification technique for danger classes of coal and gas outburst in deep coal mines; *Safety Sci.* **48(2)** 173–178.

He X Q, Wang E Y and Liu Z T 2002 Study on electromagnetic emission characteristics of loaded rock and its applications; *Chin. J. Rock Mech. Eng.* **21** 1473–1477.

Jiang Y D, Zhao Y X, Wang H W and Zhu J 2017 A review of mechanism and prevention technologies of coal bumps in China; *J. Rock Mech. Geo. Eng.* **9** 180–194.

Jiang Y D, Pan Y S, Jiang F X, Dou L M and Ju Y 2014 State of the art review on mechanism and prevention of coal bumps in China; *J. China Coal Soc.* **39** 205–231.

Leeman J R, Scuderi M M, Marone C, Saffer D M and Shinbrot T 2014 On the origin and evolution of electrical signals during frictional stick slip in sheared granular material; *J. Geophys. Res.-Solid Earth* **119(5)** 4253–4268.

Li X L, Wang E Y, Li Z H, Liu Z T, Song D Z and Qiu L M 2016 Rockburst monitoring by integrated microseismic and electromagnetic radiation methods; *Rock Mech. Rock Eng.* **49** 4393–4406.

Li Z H, Yin S and Niu Y 2018 Experimental study on the infrared thermal imaging of a coal fracture under the coupled effects of stress and gas; *J. Nat. Gas Sci. Eng.* **55** 444–451.

Lichtenberger M 2005 Regional stress field as determined from electromagnetic radiation in a tunnel; *J. Struct. Geol.* **27(12)** 2150–2158.

Liu X F, Wang X R, Wang E Y, Kong X G, Zhang C, Liu S J and Zhao E L 2017 Effects of gas pressure on bursting liability of coal under uniaxial conditions; *J. Nat. Gas Sci. Eng.* **39** 90–100.

Liu X F and Wang E Y 2018 Study on characteristics of EMR signals induced from fracture of rock samples and their application in rockburst prediction in copper mine; *J. Geophys. Eng.* **15(3)** 909–920.

Liu X F 2008 Study on time series data mining and group recognition system of electromagnetic precursor information of rockburst, Dissertation, China University of Mining and Technology.

Lu C P, Dou L M, Zhang N, Xue J H, Wang X N, Liu H and Zhang J W 2013 Microseismic frequency-spectrum evolutionary rule of rockburst triggered by roof fall; *Int. J. Rock Mech. Min.* **64** 6–16.

Mandelbrot 1999 Fractal objects (in Chinese), World Publishing Corporation, Beijing.

Mastrogiannis D, Antsygina T N, Chishko K A, Mavromatou C and Hadjicontis V 2015 Relationship between electromagnetic and acoustic emissions in deformed piezoelectric media: Microcracking signals; *Int. J. Solids Struct.* **56–57** 118–125.

Ni H Y and Liu X L 2005 Fractal characteristics and *R/S* analysis of time series of natural hazards; *J. Nat. Disasters* **14** 37–41.

Price C P and Newman D E 2001 Using the *R/S* statistic to analyze AE data; *J. Atmos. Sol-Terr. Phy.* **63(13)** 1387–1397.

Rabinovitch A , Frid V and Bahat D 2017 Directionality of electromagnetic radiation from fractures; *Int. J. Fracture* **204(2)** 239–244.

Song D Z, Wang E Y, Li Z H, Qiu L M and Xu Z Y 2017 EMR: An effective method for monitoring and warning of rockburst hazard; *Geomech. Eng.* **12** 53–69.

Sun Q and Zhu S 2014 Wave velocity and stress/strain in rock brittle failure; *Environ. Earth Sci.* **72(3)** 861–866.

Wang E Y, Jia H L, Song D Z, Li N and Qian W H 2014 Use of ultra-low-frequency electromagnetic emission to monitor stress and failure in coal mines; *Int. J. Rock Mech. Min.* **70(70)** 16–25.

Wang E Y, He X Q and Liu Z T 1998 *R/S* statistic rule of EME during deformation and fracture of coal and rock; *J. China Univ. Min. Technol.* **27(4)** 349–351.

Wang X R, Wang E Y, Liu X F, Wang H, Li X L and Li D X 2017a Experimental study on the static loading rate effects of sandstone specimen containing pre-existing echelon cracks; *J. China Coal Soc.* **42(10)** 2582–2591.

Wang X R, Wang E Y, Liu X F, Li X L, Zhang X, Zhang C and Kong B 2017b Experimental research of the AE responses and fracture evolution characteristics for sand paraffin similar material; *Constr. Build Mater.* **132** 446–456.

Wang X R, Liu X F, Wang E Y, Zhang C, Jia H S and Li D X 2018a The time-space joint response characteristics of AE-UT under step loading and its application, Shock Vib., Vol. 2018, Article ID 6210594, 11p.

Wang X R, Wang E Y, Liu X F, Li X L, Wang H and Li D X 2018b Macro-crack propagation process and corresponding AE behaviors of fractured sandstone under different loading rates; *Chin. J. Rock Mech. Eng.* **37(6)** 1446–1458.

Wang Y C, Chang N B and Lee T Y 2008 Nonlinear time series analysis of ground-level ozone dynamics in Southern Taiwan; *J. Environ. Manage.* **87** 405–414.

Zhang Z B, Wang E Y, Chen D, Li X L and Li N 2016 The observation of AE events under uniaxial compression and the quantitative relationship between the anisotropy index and the main failure plane; *J. Appl. Geophys.* **134** 183–190.

Zhang Z B, Wang E Y and Li N 2017 Fractal characteristics of acoustic emission events based on single-link cluster method during uniaxial loading of rock. *Chaos Soliton Fract.* **104** 298–306.

Zhang Z B, Wang E Y, Li N, Li X L, Wang X R and Li Z H 2018 Damage evolution analysis of coal samples under cyclic loading based on single-link cluster method; *J. Appl. Geophys.* **152** 56–64.

Zhang Z, Wang E, Zhang Y, et al. 2019 Analysis on the time-frequency characteristics of ultrasonic waveform of coal under uniaxial loading. *Fractals.* **27(06)** 1950100

Corresponding editor: Munukutla Radhakrishna